Volume 52 | Number 71 | 14 September 2016 | Pages 10699–10806

ChemComm

Chemical Communications

www.rsc.org/chemcomm

ISSN 1359-7345

ROYAL SOCIETY OF CHEMISTRY

COMMUNICATION

Jun Liang, Feng Pan *et al.*

A novel p-type and metallic dual-functional Cu–Al_2O_3 ultra-thin layer as the back electrode enabling high performance of thin film solar cells

175 YEARS

ChemComm

COMMUNICATION

View Article Online
View Journal | View Issue

Cite this: *Chem. Commun.*, 2016, 52, 10708

Received 23rd May 2016,
Accepted 28th June 2016

DOI: 10.1039/c6cc04299f

www.rsc.org/chemcomm

A novel p-type and metallic dual-functional Cu–Al_2O_3 ultra-thin layer as the back electrode enabling high performance of thin film solar cells†

Qinxian Lin,‡ Yantao Su,‡ Ming-Jian Zhang,‡ Xiaoyang Yang, Sheng Yuan, Jiangtao Hu, Yuan Lin, Jun Liang* and Feng Pan*

Increasing the open-circuit voltage (V_{oc}) along with the fill factor (FF) is pivotal for the performance improvement of solar cells. In this work, we report the design and construction of a new structure of CdS/CdTe/Al_2O_3/Cu using the atomic layer deposition (ALD) method, and then we control Cu diffusion through the Al_2O_3 atomic layer into the CdTe layer. Surprisingly, this generates a novel p-type and metallic dual-functional Cu–Al_2O_3 atomic layer. Due to this dual-functional character of the Cu–Al_2O_3 layer, an efficiency improvement of 2% in comparison with the standard cell was observed. This novel dual-functional back contact structure could also be introduced into other thin film solar cells for their efficiency improvement.

Although emerging CdTe based thin film photovoltaics (PVs) share the traditional crystalline silicon market and have advantages of competitive efficiency, long term stability and light weight,[1–3] there are numerous researchers who still explore new routes to further increase their performance.[4–9] From the view of the device structure (front electrode/n-type layer/p-type layer/back electrode) of CdTe thin film solar cells, designing novel structures for the back electrode in order to increase the ability to collect and transport photon-generated holes is an important route for the performance improvement. In CdTe thin film solar cells, the CdTe material has a higher work function (5.5 eV) than most metals, such as Al, Ag, Mo and Zn. Accordingly, the natural contact between the CdTe layer and various metals would produce a high Schottky barrier, which always leads to a "roll-over" phenomenon in the photocurrent density–voltage (J–V) characteristics. This phenomenon greatly decreases the open-circuit voltage (V_{oc}) and fill factor (FF), and so the device performance finally deteriorates.[10] To solve this problem, the common method is to introduce a back contact layer with an appropriate work function on the CdTe layer to decrease the back contact potential barrier. So far, there is much research focusing on Cu-containing materials, such as ZnTe:Cu, Cu_2S, Cu_9S_5, Cu nanowire graphene slurry, *etc.*[11–15] These Cu-containing materials could form a degenerate heavy p+ dopant in the adjacent CdTe layer and generate a CdTe/Cu_xTe interface, which would greatly improve the hole collecting ability of the back electrode and increase the J_{sc}.[10] However, this method always brings other problems. The element Cu has a great mobility in the CdTe layer, and it diffuses easily into the p–n junction region. This will result in the decrease of V_{oc} and FF, and the performance of solar cell will greatly deteriorate.[16,17] Consequently, controlling the Cu diffusion in the CdTe layer is extremely important in order to get high-performance solar cells.[18]

In our previous work, we demonstrated that CdTe solar cells based on an ultra-thin Al_2O_3 layer prepared using atomic layer deposition (ALD) displayed superior performance due to the optimized rectification and tunnelling effects.[19] However, the short circuit current (J_{sc}) decreased slightly due to the rectification effect of the ALD-Al_2O_3 layer compared with that of the standard cell. Moreover, the Cu film on the CdTe layer could easily diffuse into the p–n junction region, so as to deteriorate the device performance and reduce the cell stability. In another study, we found an appropriate p-type semiconductor (digenite Cu_9S_5 nanocrystalline film) to act as the back electrode to match with the p-type CdTe (p-type (CdTe) + p-type (Cu_9S_5), called the p + p model), which produced a good Ohmic contact at the back electrode and a high-performance CdTe thin film solar cell was achieved.[14]

We noted that Cu and Al_2O_3 could interdiffuse at the interface to form a p-type Cu–Al_2O_3 semiconductor film after annealing.[20–22] In this paper, we report the design and construction of a new structure of CdS/CdTe/Al_2O_3/Cu using the ALD method. On one hand, we hope to control Cu diffusion into the CdTe layer using the Al_2O_3 film. On the other hand, the p-type Cu–Al_2O_3 layer after annealing might be beneficial for hole transportation and could improve the cell efficiency.[23] Surprisingly, the Cu–Al_2O_3 layer was found to be a p-type and metallic dual-functional layer. It not only increased the V_{oc} and FF due to the p + p (p-type (CdTe) + p-type (Cu–Al_2O_3)) model with favourable

School of Advanced Materials, Peking University Shenzhen Graduate School, Shenzhen 518055, China. E-mail: panfeng@pkusz.edu.cn, liangjun@pkusz.edu.cn

† Electronic supplementary information (ESI) available. See DOI: 10.1039/c6cc04299f

‡ Qinxian Lin, Yantao Su and Ming-Jian Zhang contributed equally to this work.

energy level matching at the back electrode, but also avoided the decrease of the J_{sc} because of its unique metallic conductive property. In addition, the Cu–Al_2O_3 layer effectively controlled the Cu diffusion and helped to implement the optimal Cu distribution in the CdTe layer, which greatly increased the quantum efficiency in the shorter wavelength range of 500–600 nm. Finally, taking into account the multiple advantages of the novel dual-functional Cu–Al_2O_3 layer, an efficiency improvement of 2% in comparison with the standard cell was achieved.

The new device structure of FTO/CdS/CdTe/Al_2O_3/Cu/Au is presented in Fig. 1a. Accordingly, four cells with Cu films of different thicknesses (3, 6, 9 and 15 nm) were fabricated, and the standard cell (STD) was also prepared for reference. The optimized thickness of the Al_2O_3 film was found to be around 2 nm, because a thicker Al_2O_3 layer would greatly hinder the Cu diffusion (Tables S2 and S3, ESI†). The cross-sectional image of the CdTe cell was characterized using SEM (Fig. 1b). The thickness of the CdTe layer and the size of the CdTe grain could be estimated as 4–5 μm and 1–2 μm, respectively. These cells were all annealed at the optimized conditions (250 °C, 30 min in the glovebox).

J–V characteristics were measured for all these cells as shown in Fig. 1c. When the thickness of the Cu film is 9 nm, the best efficiency (13.0%) is obtained which is nearly 2% higher than that (11.2%) of the standard cell. As shown in the inset of Fig. 1c, the *J–V* curve presents a "roll-over" phenomenon when the thickness of the Cu film is 3 nm. It might be due to the imperfect Cu_xTe layer caused by the insufficient Cu diffusion into CdTe layer. In contrast, a "cross-over" phenomenon is observed when the thickness of the Cu film gets to 15 nm, which might be due to the excessive Cu diffusion into the p–n junction.[17] The detailed photovoltaic parameters are listed in Table S1 (ESI†) and plotted in Fig. 1d. It is clear that all the photovoltaic parameters, including V_{oc}, J_{sc}, FF and power conversion efficiency (PCE), increase with the increasing thickness of the Cu film, and reach their maximums when the thickness of the Cu film is 9 nm. In the best case, the V_{oc} and FF are both larger than those of the standard cell, and the J_{sc} value is nearly equal to that of the standard cell. Consequently, we could conclude that the improvement in PCE was due to the increase of V_{oc} and FF when retaining the high J_{sc}.

To get insight into the relationship between the improved performance and the properties of the Cu–Al_2O_3 film after annealing, a device with a typical metal–insulator–semiconductor structure was designed as shown in the inset of Fig. 2a. It was composed of FTO/Cu/ALD-Al_2O_3/40 nm insulation layer (Al_2O_3)/Au. Its capacitor character was evaluated at room temperature using high frequency (1 MHz) CV hysteresis curves. The gate bias was swept from inversion to accumulation (forward sweep: −1.5 to 1.5 V). As shown in Fig. 2a, the capacity decreases as the voltage increases, which demonstrates that there is a p-type semiconductor layer forming under the insulation layer.[24,25] The result is consistent with the process of Cu + O → Cu_2O and Cu_2O + Al_2O_3 → $CuAlO_2$,[26] and the mechanism is shown in Fig. S4 (ESI†). Considering the similar bond lengths of Cu–O (1.866 Å) and Al–O (1.911 Å), we guess that the plentiful Cu atoms would take the place of Al atoms, and produce the p-type Cu_xAlO_2.

In order to evaluate the electroconductive property of this annealed Cu–Al_2O_3 film, a device, whose structure is shown in the top left of Fig. 2b, was designed. The thickness of the Al_2O_3 film was fixed as 2 nm, and the thickness of the Cu film was adjustable (3, 6, 9 and 15 nm). Their *I–V* curves were measured in the voltage range of −1.0 to 1.0 V (Fig. 2b). When the thickness of the Cu film was 3 nm, the blue line is not a straight line,

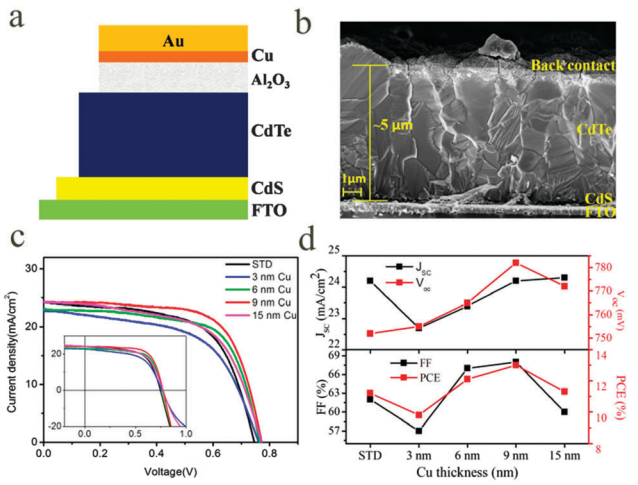

Fig. 1 (a) The design of a device structure for a CdTe solar cell; (b) cross-sectional SEM image of the CdTe solar cell; (c) *J–V* characteristics of CdTe solar cells with different Cu thicknesses on 2 nm ALD-Al_2O_3, the inset is the *J–V* characteristics of CdTe solar cells in a range of −0.2–1 V; (d) evolution of the photovoltaic parameters, including J_{sc}, V_{oc}, FF and the PCE for the solar cells with different Cu thicknesses.

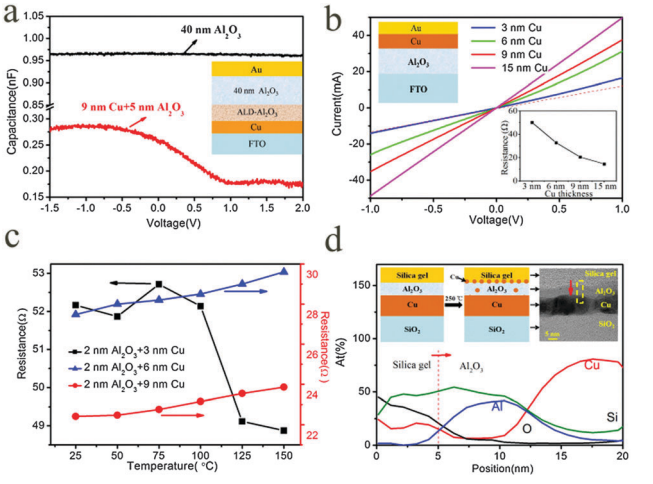

Fig. 2 (a) The CV characterization result. The inset is the device structure for the capacitance–voltage (CV) measurement; (b) *I–V* curves of 2 nm Al_2O_3 devices, the top left shows the device structure for voltage current characteristic (*I–V*) measurement, the bottom right shows the resistance of the devices with Cu of various thicknesses; (c) the temperature-dependant resistance of the devices with Cu of various thicknesses; (d) the EDX linescan curves of TEM for the Cu–Al_2O_3 thin film; the top left shows the schematic of the Cu diffusion procedure through the Al_2O_3 film and the top right shows the TEM image of the Cu–Al_2O_3 film.

which might be due to a small rectification effect and is consistent with our previous work.[19] Correspondingly, the resistance *versus* thickness curve is plotted in the inset of Fig. 2b. When the thickness of the Cu film is more than 6 nm, the *I–V* curve is straight and the resistance is very low (33–14 Ω), showing a good Ohmic contact between the Cu–Al_2O_3 film and the Au electrode. The varied-temperature resistances were further measured as shown in Fig. 2c. Remarkably, the device resistance linearly increases with the increasing temperature when the thickness of the Cu film is 6 and 9 nm. They both present a unique metallic conductive property, and the temperature coefficients of their resistance are both estimated as 6.1×10^{-4} °C^{-1} by calculating the slopes of two lines.[27] Moreover, the device resistance with a 9 nm-thick Cu film is always lower than that with a 6 nm-thick Cu film at the same temperature. Based on the analysis above, a Cu–Al_2O_3 layer with an excellent metallic conductive property after annealing was obtained when the thickness of the Cu film was 9 nm. This excellent conductive property might be beneficial to the transport and collection of photogenerated holes, and leads to a high-performance solar cell. In contrast, when the thickness of the Cu film is 3 nm, the device resistance doesn't increase with increasing temperature, and implies that it shows a kind of semiconductive property.

In order to verify the effect of Al_2O_3 on the controllable Cu diffusion, we designed and constructed a device to verify the Cu diffusion through the Al_2O_3 thin film at 250 °C as shown in Fig. 2d. The EDX linescan of TEM was performed to observe the element distribution in the cross section of the device. Obviously, the Cu content in the silica gel layer is higher than in the Al_2O_3 thin film, which means Cu can diffuse through the Al_2O_3 thin film. Moreover, the Cu content showed a gradient decrease trend at the Cu/Al_2O_3 interface, and then kept a constant level in the Al_2O_3 thin film. This indicated that Cu could be embedded in the Al_2O_3 thin film to form a p-type and metallic Cu–Al_2O_3 layer (Fig. 2a and c). In addition, it also indicated that the Al_2O_3 film could effectively control the Cu diffusion. This phenomenon is in line with our initial prediction.

Carrier lifetime is an important parameter to reflect the recombination level of photo-generated carriers in solar cells. In order to quantitatively evaluate the enhancement of carrier lifetime in the solar cells above, small-amplitude intensity-modulated photovoltage spectroscopy (IMVS) was carried out under a 560 nm light source (Fig. 3a). The back contact hole injection lifetime could be extracted from the formula, $\tau = (2\pi f_{max})^{-1}$, where τ is the carrier lifetime and f_{max} is the maximum response frequency.[28,29] As shown in Fig. 3b, the carrier lifetime of these cells are monotonically increasing until the thickness of the Cu film gets to 9 nm, which is consistent with the tendency of various photovoltaic parameters (Fig. 1d). This phenomenon could be explained by the controllable Cu diffusion *via* the ALD-Al_2O_3 film and the improved carrier transport ability by the annealed Cu–Al_2O_3 layer. When the thickness of the Cu film is not enough (3 nm), the Cu_xTe back contact could not be constructed well, and the photogenerated holes could not be efficiently transported to the back electrode,

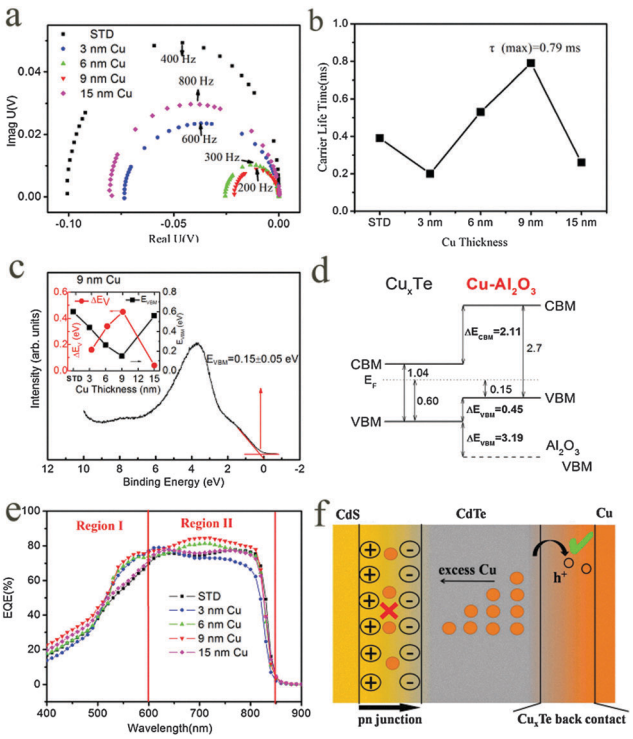

Fig. 3 (a) Typical IMVS responses for CdTe thin film solar cells, the maximum response frequency of the optimized 9 nm Cu solar cell is 200 Hz; (b) the lifetime of carriers in the CdTe solar cell according to the calculated IMVS parameters – the highest lifetime is 0.79 ms in the cell with 9 nm of Cu; (c) valence band spectrum for the optimized 9 nm Cu cell, the top left inset shows the VBM and E_{VBM} values *versus* the thickness of the Cu films; (d) energy band diagram of the CdTe/Cu–Al_2O_3 interface. The valence and conduction band offsets are represented. All of the values are given in eV; (e) EQE of the CdTe solar cell with different Cu thicknesses on 2 nm ALD-Al_2O_3; (f) the schematic diagram of the Cu diffusion mechanism in the CdTe solar cell.

resulting in a shorter hole lifetime than that of the standard cell. When the thickness of the Cu film is around 6 and 9 nm, the Cu_xTe back contact could be efficiently constructed by Cu diffusion while not damaging the p–n junction, so the hole lifetimes are longer than the standard one. When the thickness of the Cu film increases to 15 nm, excessive amounts of Cu diffuse into the p–n junction, which results in the decrease of the carrier lifetime.

To obtain the energy band structure of both the Cu–Al_2O_3 and Cu-doped-CdTe (Cu_xTe) regions around the CdTe/Cu–Al_2O_3 interface, the normalized valence band spectra for the solar cells above are presented in Fig. 3c and Fig. S8 (ESI†). In Fig. S8a (ESI†), the valence band maximum (VBM) of the CdTe surface can be determined as E_{VBM} = 0.60 eV using the linear extrapolation method. Similarly, the VBM values of the different annealed Cu–Al_2O_3 films were also obtained. The VBM value of the Cu–Al_2O_3 film in the optimized 9 nm-Cu cell is determined as E_{VBM} = 0.15 eV (Fig. 3c). All the VBM values are shown in the upper left inset of Fig. 3c, where the minimum VBM value emerges when the thickness of the Cu film is 9 nm. Using the values obtained, the offset between the valence band positions of Cu_xTe and Cu–Al_2O_3 is derived as 0.45 eV (ΔE_{VB} = 0.45 eV) at the

CdTe/Cu–Al_2O_3 interface in the optimized 9 nm-Cu cell. The ΔE_{VB} values for all the cells are also shown in the Fig. 3c inset, where the 9 nm-Cu cell has the maximum ΔE_{VB} value. In order to obtain the conduction band offset (ΔE_{CB}), the band gaps of Cu_xTe and Cu–Al_2O_3 are needed. The band gap is 1.04 eV for the Cu_xTe layer,[30,31] and the band gap of the Cu–Al_2O_3 layer is obtained as 2.7 eV from the UV-Vis transmission spectra in Fig. S7 (ESI†). So a conduction band offset of ΔE_{CB} = 2.11 eV is estimated in the best cell. The energy band diagram of the CdTe/Cu–Al_2O_3 interface can be established as shown in Fig. 3d. The values of E_{VBM}, ΔE_{VB} and ΔE_{CB} are listed in Table S5 (and Fig. S8, ESI†) for all the cells. In the best cell, the photon-generated holes in the Cu_xTe region could easily jump over the contact potential barrier of ΔE_{VB} = 0.45 eV into the Cu–Al_2O_3 region. The energy band structures of Cu_xTe and Cu–Al_2O_3 match very well with each other (Fig. 3d), which will enhance the hole collection and transport efficiency from the CdTe layer to the Cu–Al_2O_3 layer, and improve the performance of the CdTe cells. Therefore, the high performance of the best cell partly originated from the favourable energy level matching at the CdTe/Cu–Al_2O_3 interface.

In summary, we constructed a unique device structure of Cu/Al_2O_3 as the back contact of a CdTe solar cell using ALD. Notably, the annealed Cu–Al_2O_3 film presents an excellent p-type and metallic dual-functional property, which can not only increase the V_{oc} and FF due to the p + p model with a favourable energy level, but also avoid the decrease of J_{sc} because of its metallic conductive property. Combining all these advantages in the optimal cell, the best efficiency (13.0%) was obtained, which was 2% higher than that of the standard cell. This efficiency improvement could be implemented in other thin film solar cells, like CIGS, CZTS, and α-Si thin film solar cells, if such dual-functional structures are introduced into these cells.

This work was support by the Guangdong innovative and entrepreneurial research team program (Grant No. 2013N080), the peacock plan (Grant No. KYPT20141016105435850), Shenzhen key lab (Grant No. (2012)780 and ZDSY20130331145131323), Chinese postdoctoral science foundation (Grant No. 2015M57088 2), NSFC (Grant No. 11404011), Shenzhen Science and Technology Innovation Committee Grant (Grant No. JCYJ20150331101121646, JCYJ20150331100515911, and JCYJ20150629144835001).

Notes and references

1 X. Wu, *Sol. Energy*, 2004, **77**, 803–814.
2 L. Kranz, C. Gretener, J. Perrenoud, R. Schmitt, F. Pianezzi, F. La Mattina, P. Blosch, E. Cheah, A. Chirila, C. M. Fella, H. Hagendorfer, T. Jager, S. Nishiwaki, A. R. Uhl, S. Buecheler and A. N. Tiwari, *Nat. Commun.*, 2013, **4**, 2306.
3 M. A. Green, K. Emery, Y. Hishikawa, W. Warta and E. D. Dunlop, *Prog. Photovolt.: Res. Appl.*, 2015, **23**, 805–812.
4 J. D. Major, R. E. Treharne, L. J. Phillips and K. Durose, *Nature*, 2014, **511**, 334–337.
5 Z.Y. Fan, H. Razavi, J. Do, A. Moriwaki and O. Ergen, *Nat. Mater.*, 2009, **8**, 648–653.
6 C. Li, Y. Wu, J. Poplawsky, T. J. Pennycook, N. Paudel, W. Yin, S. J. Haigh, M. P. Oxley, A. R. Lupini, M. Al-Jassim, S. J. Pennycook and Y. Yan, *Phys. Rev. Lett.*, 2014, **112**, 156103.
7 H. Bi, F. Huang, J. Liang, X. Xie and M. Jiang, *Adv. Mater.*, 2011, **23**, 3202–3206.
8 H. Dang, V. P. Singh, S. Guduru and J. T. Hastings, *Sol. Energy Mater. Sol. Cells*, 2016, **144**, 641–651.
9 H. Dang, V. P. Singh, S. Guduru, S. Rajaputra and Z. D. Chen, *Nano Res.*, 2015, **8**, 3186–3196.
10 S. G. Kumar and K. S. R. K. Rao, *Energy Environ. Sci.*, 2014, **7**, 45.
11 M. Cardona and D. Greenaway, *Phys. Rev.*, 1963, **131**, 98–103.
12 H. Lin, Irfan, W. Xia, H. N. Wu, Y. Gao and C. W. Tang, *Sol. Energy Mater. Sol. Cells*, 2012, **99**, 349–355.
13 J. Türck, S. Siol, T. Mayer, A. Klein and W. Jaegermann, *Thin Solid Films*, 2015, **582**, 336–339.
14 M. J. Zhang, Q. Lin, X. Yang, Z. Mei, J. Liang, Y. Lin and F. Pan, *Nano Lett.*, 2016, **16**, 1218–1223.
15 J. Liang, H. Bi, D. Wan and F. Huang, *Adv. Funct. Mater.*, 2012, **22**, 1267–1271.
16 J. D. Poplawsky, N. R. Paudel, C. Li, C. M. Parish, D. Leonard, Y. Yan and S. J. Pennycook, *Adv. Energy Mater.*, 2014, **4**, 1400454.
17 T. D. Dzhafarov, S. S. Yesilkaya, N. Yilmaz Canli and M. Caliskan, *Sol. Energy Mater. Sol. Cells*, 2005, **85**, 371–383.
18 X. Wu, J. Zhou, A. Duda, Y. Yan, G. Teeter, S. Asher, W. K. Metzger, S. Demtsu, S.-H. Wei and R. Noufi, *Thin Solid Films*, 2007, **515**, 5798–5803.
19 J. Liang, Q. Lin, H. Li, Y. Su, X. Yang, Z. Wu, J. Zheng, X. Wang, Y. Lin and F. Pan, *Appl. Phys. Lett.*, 2015, **107**, 013907.
20 W. Lan, J. Q. Pan, C. Q. Zhu, G. Q. Wang, Q. Su, X. Q. Liu, E. Q. Xie and H. Yan, *J. Cryst. Growth*, 2011, **314**, 370–373.
21 K. A. Rogers and K. P. Trumble, *J. Am. Ceram. Soc.*, 1994, **77**(8), 2036–2042.
22 L. Fu and H. Yang, *J. Phys. Chem. C*, 2014, **118**, 14299–14315.
23 Y. Liu, H. Cheng, M. Lyu, S. Fan, Q. Liu, W. Zhang, Y. Zhi, C. Wang, C. Xiao, S. Wei, B. Ye and Y. Xie, *J. Am. Chem. Soc.*, 2014, **136**, 15670–15675.
24 C. Ostermaier, H. C. Lee, S. Y. Hyun, S. I. Ahn, K. W. Kim, H. I. Cho, J. B. Ha and J. H. Lee, *Phys. Status Solidi*, 2008, **5**, 1992–1994.
25 Y. Xuan, H. C. Lin, P. D. Ye and G. D. Wilk, *Appl. Phys. Lett.*, 2006, **88**, 263518.
26 R. Serna, D. Babonneau, A. Suárez-García, C. N. Afonso, E. Fonda, A. Traverse, A. Naudon and D. E. Hole, *Phys. Rev. B*, 2002, **66**, 205402.
27 J. H. Mooij, *Phys. Status Solidi*, 1973, **17**, 521–530.
28 J. Kruger, R. Plass and L. M. Peter, *J. Phys. Chem. B*, 2003, **107**, 7536–7539.
29 Y. Duan, J. Zheng, M. Xu, X. Song, N. Fu, Y. Fang, X. Zhou, Y. Lin and F. Pan, *J. Mater. Chem. A*, 2015, **3**, 5692–5700.
30 S. Kashida, W. Shimosaka, M. Mori and D. Yoshimura, *J. Phys. Chem. Solids*, 2003, **64**, 2357–2363.
31 B. Späth, K. Lakus-Wollny, J. Fritsche, C. S. Ferekides, A. Klein and W. Jaegermann, *Thin Solid Films*, 2007, **515**, 6172–6174.